# X-Ray fluorescence spectroscopy and mapping using excitation from white and broad bandpass synchrotron radiation

N. Stewart McIntyre,[*a] Nathaniel Sherry,[a] Marina Suominen Fuller,[a] Renfei Feng[b] and Thomas Kotzer[c]

The bend magnet VESPERS beamline on the third generation CLS synchrotron has been equipped with capabilities for X-ray fluorescence (SXRF) excitation with micro-focussed white radiation, as well as with broad and narrow bandpass monochromatised radiation. Using the former two conditions, SXRF studies have been conducted on several reference materials and metals with known elemental concentrations. The resultant spectral line shapes have been analysed using newly developed software that facilitates ready identification of K, L and M lines present as well as their subsequent spatial mapping. Using both white and broad bandpass radiation, K lines for elements from magnesium to indium and L lines from hafnium to uranium were measured and sensitivity values (S) determined. White radiation provided much higher sensitivity for most elements, and a narrower range of S values makes it possible to use a single white radiation experiment to determine a wide range of elements in the periodic table. Additionally, the variances in S values for several low Z matrices were relatively low, thus making it possible to estimate elemental concentration ranges using a reference material.

## Introduction

Synchrotron excited X-ray fluorescence (SXRF) has become almost a routine technique for the detection of trace and minor elements in materials ranging from minerals to metals to biological tissues.[1–3] In recent years, many SXRF studies reported have used radiation in beamlines off insertion devices. The immense improvement in photon flux has naturally made such beamlines choice facilities for XRF experiments[4] and it has also been argued that the ability of such beamlines to use narrow bandpass radiation at selectable energies results in a significant improvement in the signal/background ratio obtained in XRF spectra.[5] Still, bend magnet beamlines, particularly on third generation synchrotrons, can deliver photon flux that is quite acceptable for many applications, sometimes with lower noise and spectral signatures. Moreover, the development of improved X-ray mirror optics and coatings has increased the intensity available in micro-focussed bend magnet beams.

The VESPERS beamline at the Canadian Light Source was designed to use bend magnet radiation to conduct simultaneous XRF and Laue X-ray diffraction experiments on near microns-size regions of a sample.[6] Separate alternate optical pathways provide "white" radiation and monochromatised radiation with different bandpass settings. Two sets of multilayer mirrors[7] provide bandpasses of 1% and 10%, and ⟨111⟩ silicon is used to provide an ultimate resolution of 0.01%. Using the 10% multi-layer mirror, a selective spectral region can be irradiated with a beam flux considerably higher than that obtained by more conventional narrow bandpass radiation. Excitation by white

radiation is another attractive excitation mode, provided that any background radiation from reflection and Compton scattering can be kept acceptably low using detector geometry and mathematical filtering.

In this paper, we compare the use of 10% bandpass mono-chromatisation and two modes of white radiation in the XRF excitation of a number of differing sample matrices with known compositions. The high energy mode of white light excitation available on VESPERS, is able to provide K line spectra from Mg to In, along with L line spectra of many of the higher Z elements. Identification of elemental patterns has been facilitated by the use of a newly developed software package that fits multiple peak envelopes, and filters the spectral backgrounds and noise. Although it produces lower intensity XRF spectra, the 10% bandpass mode is found to provide spectra that are some-times more accurately fitted compared to those using white radiation.

## Experimental

The geometry of the VESPERS beamline has been described in recent publications.[6,8] Briefly, two separate optical pathways are provided from the defining apertures at the upstream wall. One of these passes through a double crystal monochromator in which two multilayer stacks and a silicon (111) substrate are positioned to provide spectral bandpass energy windows of 0.01%, 1.5% and 10%.[5] The other optical pathway does not pass through the monochromator, thus producing polychromatic (white) radiation. Even the balance in this white radiation can be changed from a low energy mode favouring the lower energies from 3–12 kV (4.0 mradians mirror angle) to a high energy mode favouring energies above 12 kV (2.4 mradians mirror angle). Both monochromatic and white radiation beams are cotermi-nous and both are focussed using separate upstream 310 mm

[a]VESPERS Group, Faculty of Science, University of Western Ontario, London, Ontario, N6A 5B7, UK. E-mail: smcintyr@uwo.ca
[b]Canadian Light Source, University of Saskatchewan, Saskatoon, Saskatchewan, S7N 0X4, Canada
[c]Cameco Inc., Saskatoon, Saskatchewan, S7N 1J3, Canada

K–B mirrors and a single set of downstream 150 mm bendable K–B mirrors. The geometry of the optics allows for acceptance of photons below ∼30 kV; the photon flux from 20 to 30 kV on this bending magnet beamline rolls off rapidly in this range, but is still sufficient to excite some K line spectra above 20 kV. Three different reflective surfaces on the mirrors (Pt, Pd and Si) can be used to shape the energy distribution of the beam. Platinum coatings on all mirrors and a beam intersecting angle of 4 mradians on the upstream mirrors produce a white beam with a broad elastic energy maximum around 12 kV and an energy cut-off near 20 kV. A higher energy white radiation mode is obtained by changing the beam intersecting angle to 2.4 mradians. The photon flux with the 10% bandpass set at 15 kV has been calculated to be $5 \times 10^{10}$ photons s$^{-1}$ under current CLS operating conditions (∼200 mA ring current). Beam spot size is determined by slits that are placed at the first focus position of the double focussing beam optics. The smallest spot size used in this work was $1.0 \times 1.6$ μm for a white light beam intersecting the mirrors at 2.4 milliradians (higher energy white radiation mode).

Samples were mounted on a three way Nanomotion stage that was tilted at 45 degrees azimuthally and orthogonally to the incoming beam. The stage performs rastering patterns to allow intensity distributions to be plotted as maps, with corrections for the sample angles. XRF spectra were recorded with a SII Nanotechnology Vortex single channel 50 mm$^2$ Si drift diode (SDD) detector mounted at 45 degrees to the sample, 90 degrees to the incident beam and 3 cm distance from the sample. This SDD detector is capable of collecting very high count rates (∼600 kHz) at 0.25 μs peaking times. Such rates do cause a noticeable broadening of X-ray peaks compared to optimum resolution at a peaking time of 5 μs. This broadening can be seen in some of spectra produced by white radiation. Typically, dead time losses in these experiments were kept lower than 10%. No cover gas was used between the sample and the detector; however, the air pathway was sufficiently small that Mg, Al and Si K lines were detected from samples bearing high concentrations of these elements. Each 2000 point spectrum produced is saved for detailed analysis.

The machine-level EPICS software of the beamline was overlayed by a Beamline Control Module that was addressed by web services software called Science Studio. Science Studio allows experimenters to acquire XRF spectra and spatial distributions from a remote location. Several of the datasets shown in this work were acquired under control from, and rapidly downloaded to, the University of Western Ontario. The program "Peakaboo" is a part of the Science Studio package that allows users to identify the spectral origins of the XRF spectrum using a routine that fits all components of the K or L spectrum including escape peaks (but not pileup peaks), and then plots their spatial intensity distributions as maps. The software provides a number of mathematical filters that are used in noise reduction or in background attenuation or removal. Noise filters include moving average, fast Fourier transform (FFT) low pass, Savitsky–Golay[9] and wavelet transform.[10] Where applicable, the reach and order of the polynomial used can be altered. For the FFT low pass filter, the type of roll off and the start and end energies of the roll off can be specified. For this work a single pass of a Savitsky–Golay filter (7 order polynomial with a reach of 15) was used. This was found to have a negligible effect on the shape of the

fitted peaks. It takes 24 minutes for the Java-based software to apply a Savitsky–Golay filter to 5000 spectra acquired for an elemental distribution map, using an average dual core laptop. A parabolic filter with a variable polynomial is used to determine the position and shape of the spectral background.[11] The spectra produced are fitted with several K, L and (sometimes) M lines for each element. The line positions and relative intensities for each line series were taken from several tabulated sources.[12,13] Fits took account of details such as separations and relative intensities of Kα 1 and 2, Kβ 1, 2, and 3, Lα, Lβ 1 and 2, Lγ 1, 2, and 3 lines. For most of the K series elements from Ca to Mo, the relative intensities of α and β composite lines were checked and adjusted for our Lookup Table using metals or compounds. As well, a number of metals with strong L series spectra were analysed and the relative intensities adjusted accordingly; most (but not all) ratios were found to agree well with the tabulated sources. For fitting of the spectral peaks, a Gaussian function was used with preset widths. Thus, the identification of a particular element requires a close fit of multiple lines in the spectrum, each with its own shape. When the presence of a particular element is to be tested in the presence of overlapping lines, the unknown element's predicted spectrum is fitted to that portion of the measured spectrum which is not already accounted for by the fittings from the other elements. The fitting algorithm developed does not allow all sets of elemental peaks to be freely variable to fill the available peak intensity envelope. A criterion for introducing a new elemental fitting is that the amount of fitted signal will be limited by the least-represented line to prevent misattribution of overlapping lines. Thus, the fitting algorithm is greedy (fits against as much signal as it can) on an element-by-element basis, but not on a peak-by-peak basis. Several fitting sequences need to be tested to ensure that the solution is consistent.

The workflow on Peakaboo revolves around a single screen where choices are made concerning filters and elemental spectra to be chosen. A screenshot, seen in Fig. 1, shows a drop-down menu for spectral display options. To assist in identifying and mapping all elements in a scanned area, an average of all spectra can be displayed or one that searches for the strongest peaks in all spectra in a map. The software is particularly easy for novices to negotiate. Peakaboo software is freely available for download from: www.sciencestudioproject.com.

Samples of NIST SRM 610 and 612 glasses were purchased from SPI Supplies Inc. and were subject to a few seconds of a 5% nitric acid wash before use. A sample of NIST Montana soil 2711 was kindly provided by Dr Derek Peak of University of Saskatchewan. The compositions as determined by numerous methods are found at http://www.nist.org/. Al 6061 was obtained from machine shop stock. Alloy 600 was obtained from Chalk River Laboratories. Both of the latter metal alloys were analysed by Activation Laboratories in Dundas, Ontario using ICP-MS. The results of these analyses are available in the archives of this Journal.

## Results and discussion

The XRF spectra for NIST SRM 610 sodium calcium silicate glass reference material are shown in Fig. 2a and b, as obtained using a micro-beam of unfiltered white radiation in the high energy mode. Intensities displayed in linear form represent all
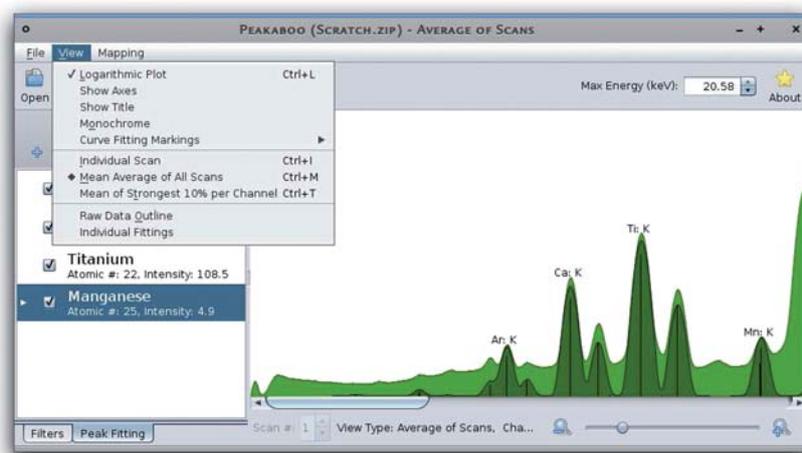
**Fig. 1** Screenshot of the Peakaboo data display page.

additive elements from scandium to indium along with the heavy element additives tungsten, lead, bismuth and uranium. All peaks shown were able to be fitted with K or L line components for these elements. Of the 61 elements added to the glass at the nominal 500 µg g⁻¹ concentration level, 30 were able to be fully resolved by the software. During the fitting process, it was not possible to fit all elements at one time, due to present software limitations on the variation of the overlapping intensities for each elemental pattern. Thus, it was determined that elements with strong L patterns could usually be fitted in a separate process. Fig. 2a shows the close fit of most of the spectral profile provided by the K line components of elements from Ca to In. Fig. 2b shows the fitted L line components; those for Hf, W, Tl, Bi, Pb, Th and U were able to have their complex patterns fitted and unambiguously separated from the surrounding K line

components. Components for the lanthanide additives Nd, Th and U could be fitted but not without some loss of contribution from the surrounding K lines. The 10% bandpass mode was also used to measure the SRM 610 sample. Fig. 3a and b show separate K and L line fittings in logarithmic form for the spectrum produced for a 10% bandpass "window" centred at 25 kV. For the K lines, the somewhat enhanced sensitivity for those lines with energies closer to the irradiating energy is apparent. The L line components for elements such as U and Th appear to be better fitted than with white radiation, probably because the lower background makes it easier to resolve each L component completely.

The known (or expected) bulk concentration values in the SRM 610 reference glass were used to develop sensitivity factors (S). S is the total K or L line intensity (above background)
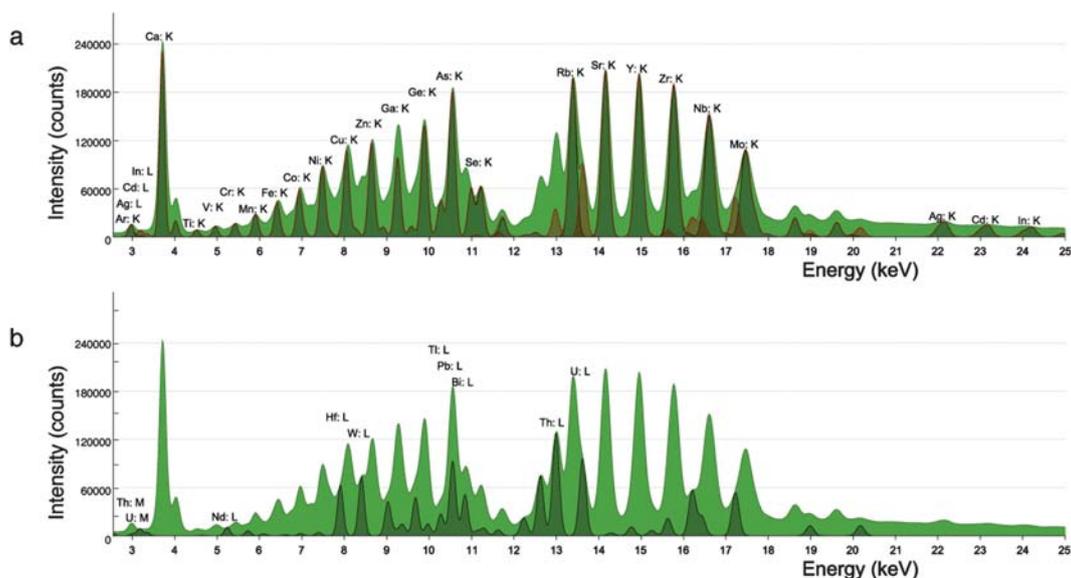


**Fig. 2** SXRF linear spectrum (3–25 keV) of reference glass SRM 610 (nominal 500 ppm additive concentrations) taken using unfiltered white radiation with a mirror angle of 2.4 mRad (high energy mode). The accumulation time was 600 s and the spectrum was mathematically filtered using a single pass Savitsky–Golay treatment. No background correction has been applied in this case. All individual components of the fit for each peak are shown under the curve along with their composite envelopes. (a) K line spectral fits for elements from Ca to In. (b) L line spectral fits for Hf, W, Pb, Bi, Th, U and Nd.
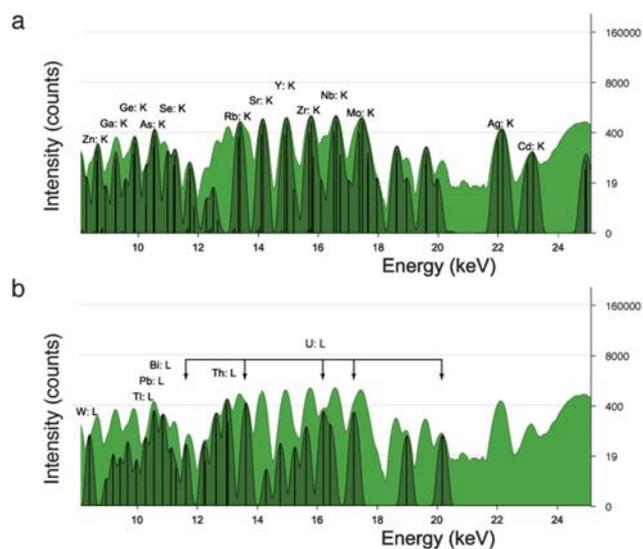
**Fig. 3** SXRF log spectrum (8–25 keV) of reference glass SRM 610 taken using radiation for a 10% bandpass monochromatisation centred at 25 keV. The accumulation time was 600 s and the spectrum was mathematically filtered using a single pass Savitsky–Golay treatment. Ninety percent of the parabolically fitted background was removed. (a) K line fits for elements from Zn to Cd (b) L line fits from W to U, showing individual lines for U. The intensity maximum around 25 keV results from an elastic peak and from Compton peaks.



**Fig. 4** Sensitivity ($S$) values (counts min$^{-1}$ mg$^{-1}$) determined for (a) K and (b) L lines for reference glass SRM 610 using high and low energy modes of white radiation and 10% bandpass monochromatised radiation centred at 20 kV, 22 kV, 25 kV and 27 kV.

produced by a fixed atom density of a particular element in a 60 second acquisition time. $S$ values can be used, along with counting statistics, to compare the effects of matrix and sample geometry on the intensity as well as to determine Minimum Detection Limits (MDL's). In Fig. 4a and b, a log plot of the $S$ factors is shown as a function of atomic number for K and L lines for both modes of white radiation, and for different exciting energies using the 10% bandpass mode. For high energy mode (2.4 mradian mirror angle) of white radiation excitation, the $S$ value increases regularly from Ti ($Z = 22$) to Cu ($Z = 29$), but in the interval from Zn to Rb ($Z = 37$) there are irregularities to the curve that result from the rather complex background in this region of the spectrum that is not completely represented by our present algorithm. Beyond rubidium, $S$ values roll off gradually to the highest detectable K line (In at 24 keV), under these instrumental conditions and additive concentrations. For the lower energy mode of white light (4 mradian mirror angle), the $S$ values are slightly higher for those elements in the energy range below arsenic, but are significantly lower for the higher Z elements. For 10% bandpass excitations, the curves of $S$ values for different excitation energies decrease in value as the energy increases, because of the decreasing flux of exciting photons available as higher energies are accessed. The $S$ values for all 10% bandpass excitation conditions are considerably lower than those for the same elements excited by white radiation. However, use of the highest excitation energy allowed the K line detection range to be extended to the element tin.

Total intensity L line $S$ values for the SRM under the same white radiation and 10% bandpass conditions are shown in Fig. 4b. For elements below W ($Z = 75$), $S$ values were not c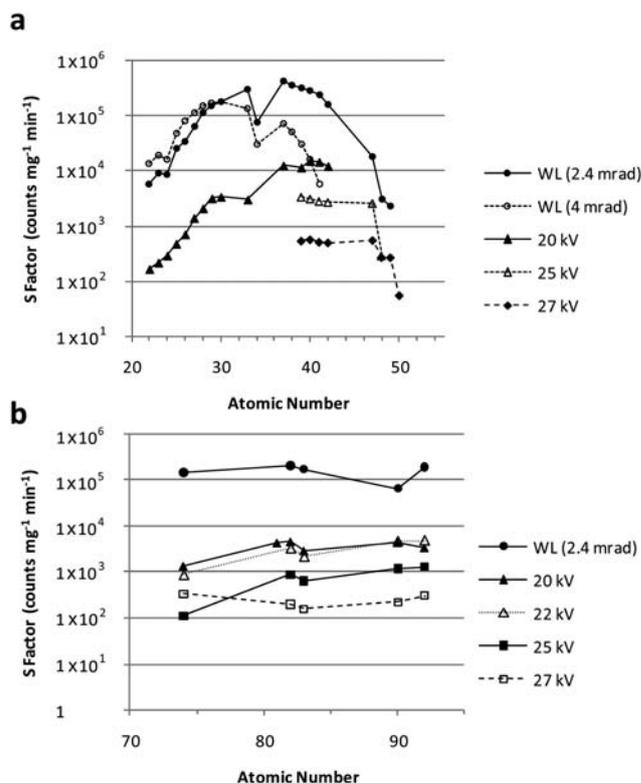onsistent, since quantitative measurements of the L lines of these elements in this matrix were complicated by the presence of strong K lines that obscured at least some of their line structure. For the heavier elements measured, the L line $S$ values are quite constant.

Minimum detection limits (MDL's) can be determined for particular elements based on our measurements of RMS noise in regions between peaks in this spectrum close to the As K lines. The MDL calculations involve intensity measurements only, and not the coincidence of related peak components. After Savitsky–Golay filtering, RMS noise is 90 counts for a one minute spectrum. Thus, the (3Σ) MDL in high energy white radiation for As would be 0.7 μg g$^{-1}$ for a 60 second acquisition or 30 μg g$^{-1}$ for a 5 second acquisition (more typical of counting times used in acquiring a spatial map). The analytical volume involved would be as small as 100 μm$^3$. The additive use of multiple spectral components in identifying an element not only increases the sensitivity but also provides much greater assurance that the intensity, in fact, belongs to the element in question.

A similar study was done for NIST SRM 612, a sodium silicate glass to which 60 elements had been added at a nominal concentration of 50 μg g$^{-1}$. The lack of homogeneity of this reference material has been suggested previously;[14] therefore, the spectrum obtained was a composite from spectra taken at three locations. Of the 60 elements added to the glass, 31 could be cleanly resolved using the Peakaboo analysis software and a few of the lanthanides partially resolved. Fig. 5 shows $S$ values for K lines for the low energy mode of white radiation as well as for
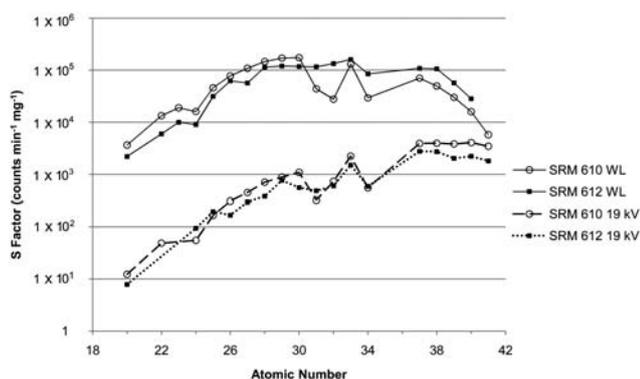
**Fig. 5** Sensitivity (*S*) values (counts min⁻¹ mg⁻¹) compared for K lines of elements detected in SRM 610 and SRM 612 using the low energy mode of white light excitation and broad bandpass monochromatisation at 19 kV.
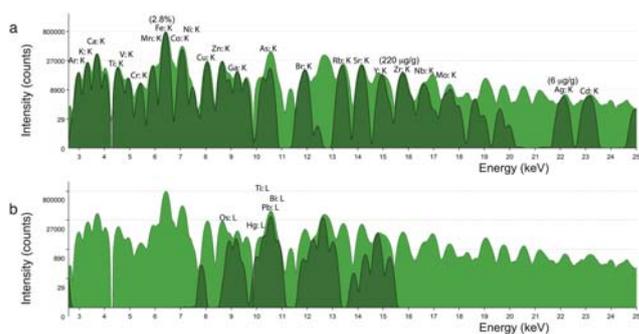


**Fig. 6** SXRF spectrum of SRM Montana Soil 2711 acquired using white radiation (high energy mode). The accumulation time was 600 seconds and the spectrum noise was filtered using a single pass Savitsky–Golay treatment. Ninety four percent of the parabolically fitted background was removed. Non-labelled peaks were found to have arisen from peak pileup from lower Z elements. Some elemental concentrations provided with the SRM are shown. (a) K line fits from 3–25 keV (b) L line fits.
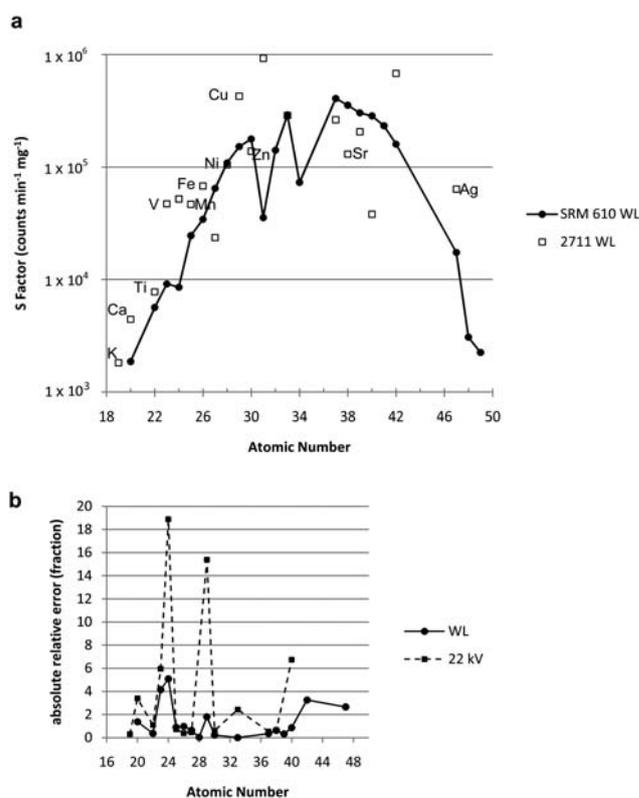
broad bandpass radiation centred at 19 kV; these are compared to those obtained for SRM 610 under the same conditions. Both sets of *S* values for SRM 612 are quite close to those for SRM 610, showing that the effects of dilution in the calcium silicate matrix are not major. For the lower Z elements in SRM 612, there is a small decrease in sensitivity that is attributed to decreased excitation of these elements from secondary radiation from higher Z elements. The *S* values for 612 elements do not show the same discontinuity in the Ga–Ge range as was found for 610. This could result from fewer background correction complexities in the more dilute 612 matrix, compared to those in 610.

SRM 612 has been previously analysed by radiation at HASYlab (beamline L)[15] and the MDL's from that work reach a minimum (maximum in sensitivity) in the broad range around $Z = 40$, similar to the maximum in *S* observed for high energy white radiation for VESPERS. However, the available energy in beamline L extended considerably higher than for VESPERS, resulting in access to K lines for higher Z elements. Based on the MDL calculations for SRM 610, using our present XRF geometry, the MDL's for VESPERS for elements near $Z = 40$, are about 5 times lower than were reported for beamline L in its condition about a decade ago.

The use of white and broad bandpass monochromatised radiation was also studied for a NIST SRM soil: 2711 (Montana soil), a soil from a region near a former mine site. Fig. 6 shows a high energy mode white radiation spectrum for the SRM 2711 soil. The K line fits show iron to be a major constituent and trace elements K lines as high as silver and cadmium can be detected. In Fig. 7a, *S* values are compared for Montana soil and SRM 610 under both white radiation and broad bandpass monochromatised radiation. For white radiation excitation, *S* values for K lines of certified concentrations for Montana soil 2711 follow a pattern that is similar to that traced by SRM 610; the average percent difference between elemental *S* values for white radiation is 140%; *i.e.* the average *S* value for 2711 is only a factor of 1.4 away from the *S* value for 610, despite a few major concentration differences. Some of the major elemental *S* value differences (see Fig. 7b) can be attributed to the secondary fluorescence contributions from the iron K line on lighter elements. The *S* value for iron with a concentration of 2.2% is





**Fig. 7** (a) K line sensitivity (*S*) values (counts min⁻¹ mg⁻¹) for elements in Montana Soil 2711 measured with both white radiation and 10% broadband monochromatisation centred at 25 kV as compared with equivalent measurements made for SRM 610. *S* values for elements with certified concentrations are identified by the elemental symbol. (b) Plot of the relative error (absolute value of fraction) of the *S* values for the Montana soil data shown in (a) compared to the equivalent SRM 610 measurements as the reference standard.

within a factor two of the value for iron in SRM 612, having a concentration of 50 µg g⁻¹. Compared to white light excitation, the *S* value differences for broadband radiation centred at 22 kV were somewhat larger.
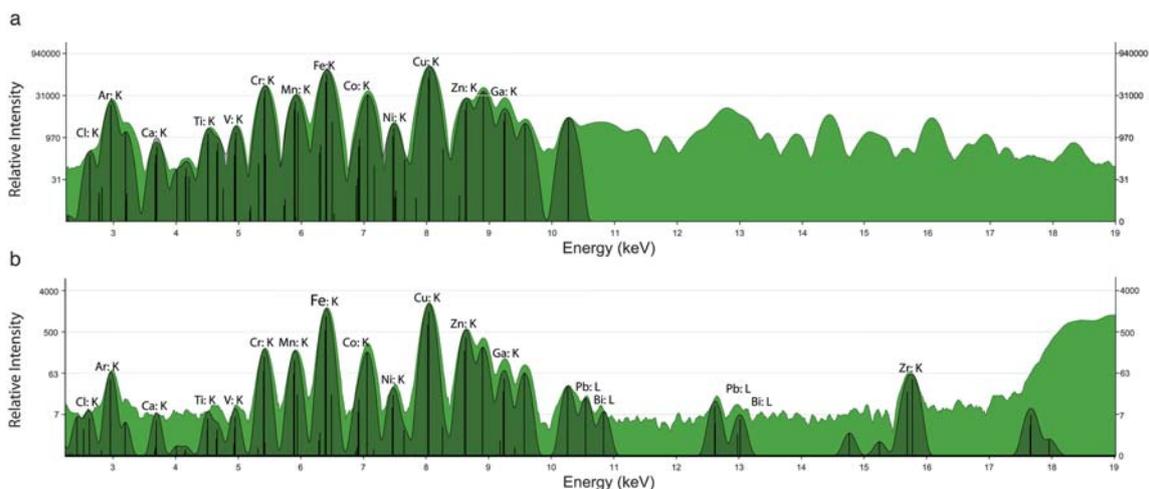
**Fig. 8** SXRF spectra of Al 6061 acquired with (a) white radiation (low energy mode) and (b) 10% broadband monochromatisation centred at 19 keV. Using white radiation all peaks above the Ga K line result from peak pileup of lower Z elements; using 10% broadband radiation such pileup is reduced and lead, bismuth and zirconium impurities are detected. Ninety percent of the parabolically fitted background was removed. Spectrum noise was filtered with a single pass Savitsky–Golay treatment.
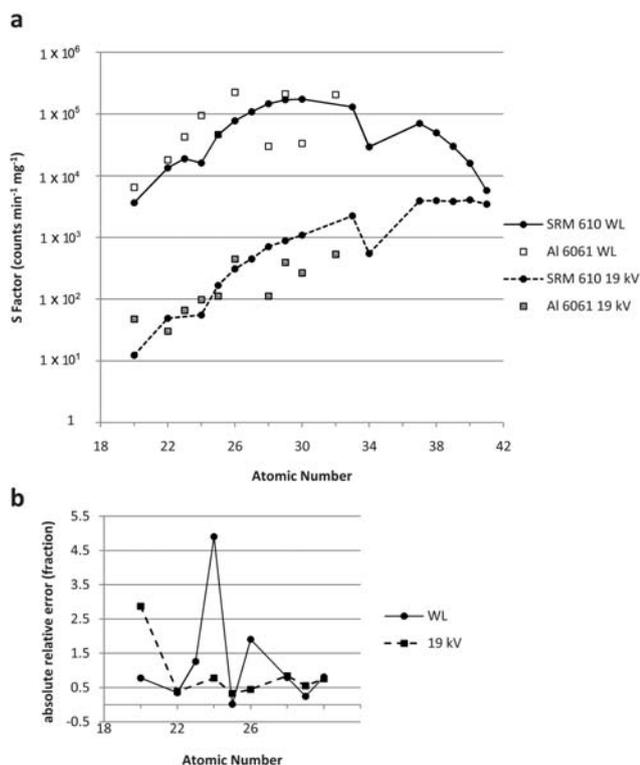


**Fig. 9** (a) K line sensitivity (S) values (counts min$^{-1}$ mg$^{-1}$) for elements in Al 6061 measured with both white radiation (low energy mode) and 10% broad bandpass monochromatisation centred at 19 kV. These are compared with equivalent measurements for SRM 610. (b) Plot of the relative error (absolute value of fraction) of the S values for the Al 6061 data shown in (a) compared to the equivalent SRM 610 measurements as the reference standard.

from Mg to Ga are detected. At energies above Ga, the background due to peak pileup from the lower Z spectra is appreciably higher than it was for the silicates previously analysed, probably the result of a higher Compton scattering component in the spectral background. By contrast, the spectrum excited by broadband monochromatised radiation (Fig. 8b) has a background in the same region that is significantly lower, thus allowing trace components of lead, bismuth and zirconium to be detected. Fig. 9a compares the S values for both excitation modes with those for SRM 610. The average percent difference between white radiation S values for 610 and those for Al 6061 is 125% (Fig. 9b). For the broad bandwidth monochromatised excitation the average differences in S values were lower.

The XRF spectrum for Alloy 600, nickel–iron–chromium alloy, was obtained using white radiation (not shown). Based on the
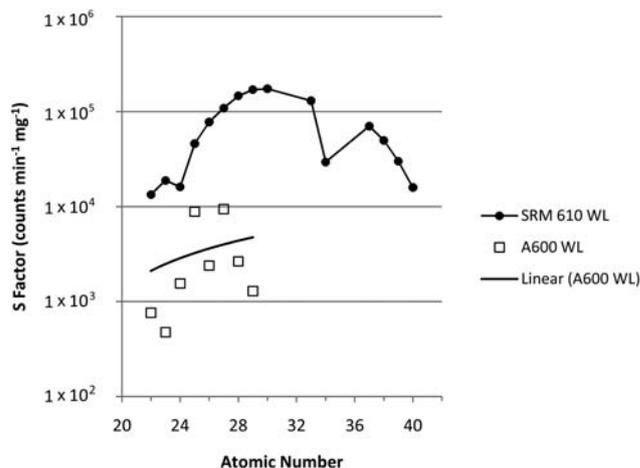
The effects of broadband and white radiation were also compared for low and medium Z metals of known composition. The spectrum of Al alloy 6061, excited by white radiation, is shown in Fig. 8a. K line peaks for constituent elements ranging



**Fig. 10** K line sensitivity (S) values (counts min$^{-1}$ mg$^{-1}$) for elements in Alloy 600 measured with white radiation (low energy mode), compared with equivalent measurements for SRM 610. The dashed line is a least squares fit of the data.
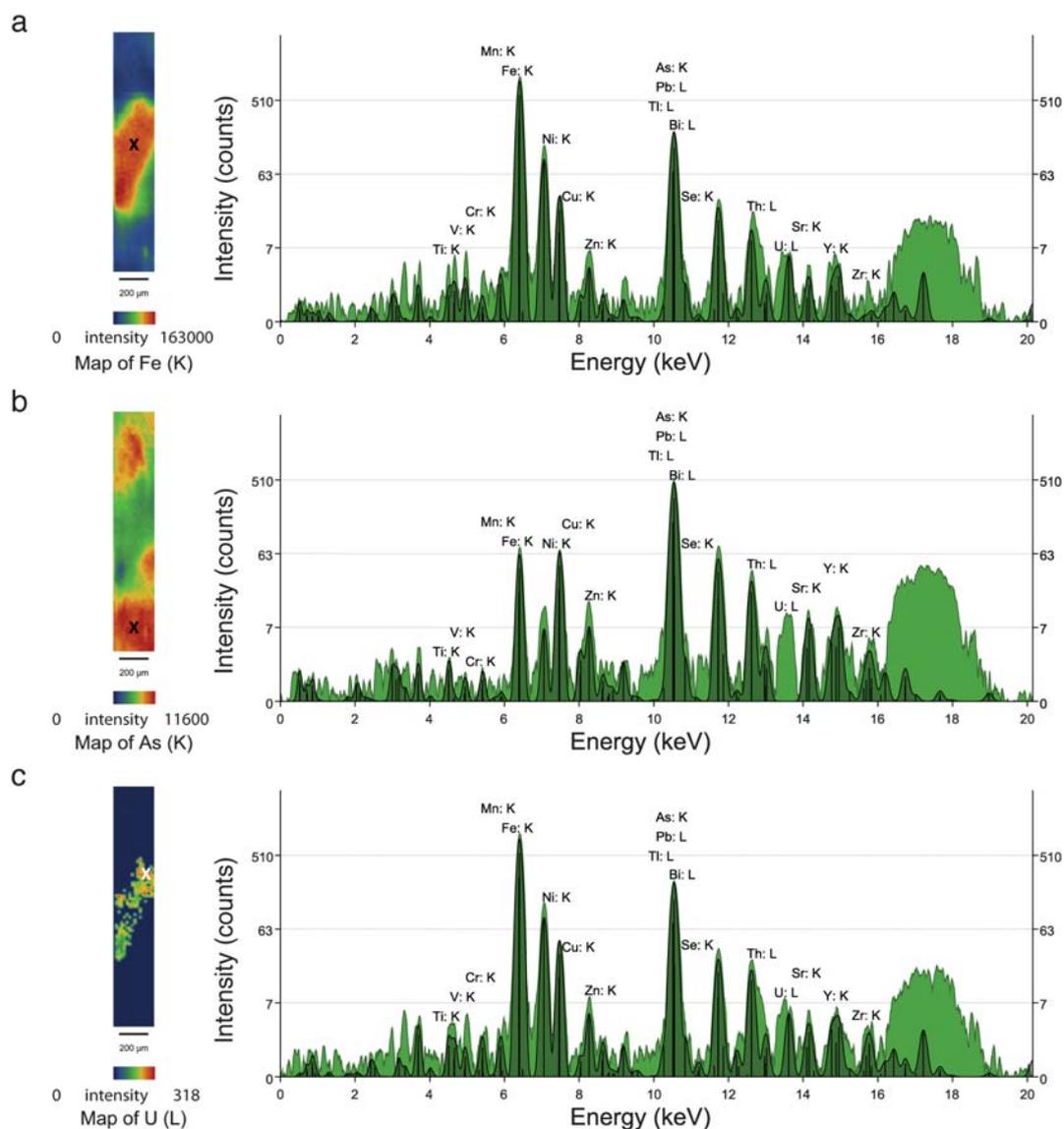
Fig. 11 Spatial distributions for three elements: Fe (a), As (b) and U (c) measured from the SXRF spectra of a uranium tailings specimen from the Athabasca Basin. The area scanned is 800 × 250 microns and the dwell time per pixel was 3 seconds. Spectra were excited using broad bandpass monochromatisation centred at 17 keV and with a spot size of 5 microns for this work only. Spectra of local spots on the sample (marked with an X) are shown in logarithmic format.

analysed concentrations for a number of elements in the matrix, $S$ values were computed and are compared to those for SRM 610 in Fig. 10. By contrast to the previous examples for low Z matrices, the $S$ values for Alloy 600 followed a trend line that was at least a factor of ten below that for SRM 610. This probably results from the much higher absorption of the primary photons by the higher Z metal matrix, and thus shows that SRM 610 is not at all suitable as an approximate reference for this alloy, and presumably any other medium or high Z matrices.

A broad bandpass monochromatised beam was used to acquire a spatial map for a uranium tailings specimen from the Athabasca basin in Saskatchewan, Canada. The sample was known to contain, among other elements, arsenic oxides and sulfides, along with iron and calcium oxides. A series of XRF spectra were acquired in a 100 × 50 grid with a step size of 2 microns and

a collection time of 3 seconds. The noise in each spectrum was reduced with a single pass Savitsky–Golay filter. A composite spectrum was derived from spectra collected for each point, and this was used to fit and identify K and L line structures for numerous elements in the sample. The total intensity for each element line was used to plot a map whose pixel intensities were scaled to show the total range of intensities collected within the mapped area. In Fig. 11a maps of iron, arsenic and uranium distributions are shown, along with spectra that are specific to regions where the element is near its maximum intensity. Iron and arsenic appear to dominate complementary parts of the map, but there is in fact, significant arsenic intensity within the iron-rich area, as shown by the spectrum. Uranium is distributed within part of the phase that is more highly enriched in iron, particularly in a small region near the top. Iron can be an interferent to the
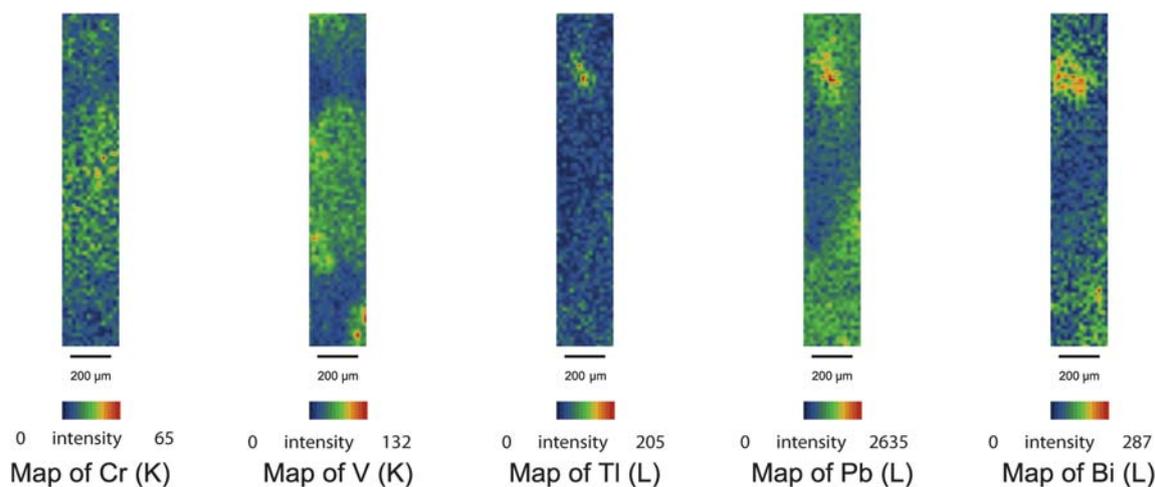
**Fig. 12** XRF maps for the distributions of 5 additional elements: Cr, V, Tl, Pb, and Bi.

detection of uranium because of the proximity of a Fe Kα pileup peak at an energy just below the U Lγ peak at 13.2 keV. This interference is mostly avoided since the entire set of five uranium L peaks is required to authenticate the presence of a uranium L emission. The fact that the distribution of low intensity uranium signal differs from that of iron shows that the procedure is sound. Fig. 12 shows the distribution of several other first row transition elements and higher Z elements. The maps for chromium and vanadium K lines follow the outline of the iron-rich region, but their intensity distributions differ in detail. Maps for the L lines of Tl, Pb and Bi all show small scale enrichments within the same region of a region enriched in arsenic. The arsenic Kα line represents an interferent to the Pb L line, but it can be seen here that this follows quite different intensity distributions because of the requirement that all Pb L lines be fitted.

The white radiation from the VESPERS beamline provides respectable sensitivities for a majority of elements in the periodic table simultaneously. Most of these, from magnesium to molybdenum and beyond are detected using a spectral fit of the K lines produced. Some of the heavier elements, particularly those above tungsten can be detected using a fitting of their L lines. Lines for elements from Sn–Ba would only be detectable under the unusual circumstances where the overlapping K lines of the first row transition elements were not present. For this reason, XRF studies of these elements would be better carried out on a higher energy beamline with tuneable radiation to excite K lines of a particular element.

The comparable S values obtained for elements in several different low Z matrices suggest that an initial white radiation XRF measurement using SRM 610 could provide very approximate concentration ranges for most elements in such matrices, to be followed by a second calibration using a reference material with elemental concentration values closer to those for the unknown matrix.

There are still advantages to the use of broad bandpass monochromatised radiation, especially where a limited number of elements are to be determined. The sometimes better signal/background allows better fitting of the entire peak shape. In addition, use of the higher energy excitation reduces the possibility of peak pileup from intensities of lower Z elements.

## Conclusions

(1) White light excitation conditions on the VESPERS beamline have been identified that will allow excitation of K and L spectra for a reasonably wide range of trace and major elements in several different matrices. Mathematical filters have helped to reduce noise and spectral backgrounds. The elemental sensitivity factors produced by the white radiation are, in general, many times higher than those obtained using broadband monochromatised radiation. Sensitivity values for the same element usually fall within a factor of three of each other for several low Z matrices (silicates or elemental aluminium), even where elemental concentrations differed significantly.

(2) Excitation using broadband monochromatisation sometimes provides somewhat narrower peaks and lower backgrounds, thus allowing better discrimination of a particular element where the exciting line is positioned just above the absorption edge.

## Acknowledgements

## References

1 M. A. Marcus, A. A. MacDowell, R. Celestre, E. Domning, K. Franck, A. Manceau, G. Morrison, T. Miller, H. A. Padmore and R. E. Sublett, *J. Synchrotron Radiat.*, 2004, **11**, 239–247.
2 F. Adams, K. Janssens and A. Snigerev, *J. Anal. At. Spectrom.*, 1998, **13**, 319–331.

3 S. Bohic, A. Simionovici, A. Snigrev, R. Ortega, G. Deves, D. Heymann and C. G. Schroer, *Appl. Phys. Lett.*, 2001, **78**, 3544–3546.

4 Y. Nishiwaki, T. Nakanishi, Y. Terada, T. Ninomiya and I. Nakai, *X-Ray Spectrom.*, 2006, **35**, 195–199.

5 F. Adams, L. Vincze and B. Vekemans, Synchrotron Radiation for Microscopic X-ray Fluorescence Analysis, in *X-Ray Spectrometry: Recent Technological Advances*, ed. K. Tsugi, J. Injuk and R. Van Grieken, John Wiley and Sons, 2004, pp. 343–353.

6 R. Feng, A. Gerson, G. Ice, R. Reininger, B. Yates and S. McIntyre, *AIP Conf. Proc.*, 2007, **879**, 872–874.

7 R. Feng, Y. Platonov, D. Broadway, G. Ice, A. Gerson and S. McIntyre, *Proc. SPIE-Int. Soc. Opt. Eng.*, 2008, **7077**, 70771.

8 R. Feng, W. Doulton, R. Igarashi, G. Wright, M. Bradford and N. S. McIntyre, SRI Proceedings, in press.

9 A. Savitsky and M. J. E. Golay, *Anal. Chem.*, 1964, **36**, 1627–1639.

10 S. Mallett, *A Wavelet Tour of Signal Processing*, Academic Press, New York, 1999, p. 199.

11 P. Collela and P. R. Woodward, *J. Comput. Phys.*, 1974, **54**, 174.

12 M. Kraus, *J. Phys. Chem. Ref. Data*, 1979, **8**, 307–327.

13 National Physical Laboratories, Kaye and Laby Tables, Chap. 4.2.1. X-Ray Absorption Edges, X-ray Fluorescence lines and Fluorescence Yields, http://www.Kayelaby.npl.co.uk.

14 L. Kempenaers, K. Janssens, L. P. Jochum, L. Vincze, B. Vekemans, L. Somogyi, M. Drackopoulis and F. Adams, *J. Anal. At. Spectrom.*, 2003, **18**, 350–357.

15 L. Vincze, A. Somogni, J. Osan, B. Vekemans, S. Torok, K. Janssens and F. Adams, *Anal. Chem.*, 2002, **74**, 1128–1135.

This journal is © The Royal Society of Chemistry 2010

*J. Anal. At. Spectrom.*, 2010, **25**, 1381–1389 | 1389